Yadav et al. Egyptian Journal of Neurosurgery (2024) 39:12
https://doi.org/10.1186/s41984-024-00277-6

Egyptian Journal of Neurosurgery

RESEARCH

Open Access

Morphometric analysis of posterior cranial fossa and foramen magnum and it's clinical implications in craniovertebral junction malformations: a computed tomography based institutional study in a tertiary care hospital of northern part of India

Vikrant Yadav[1*], Ravi Shankar Prasad[1], Anurag Sahu[1], Manish Kumar Mishra[1] and Ravi Shekhar Pradhan[1]

Abstract

Background The posterior cranial fossa (PCF) and the foramen magnum (FM) are the critical anatomical components of the craniovertebral junction region, which comprise and transmit numerous vital neurovascular structures. So, a fundamental knowledge of the basic radiological anatomy of PCF and FM is of paramount importance in the evaluation of associated pathologies and approaching these areas surgically. The aim of this study is to describe different linear and angular craniometric parameters of PCF, FM and surrounding territory based on reconstructed computed tomography (CT) images.

Material and methods This study was conducted in our tertiary care hospital in northern India from the period of January 2023 to June 2023 on 120 patients, and CT screening was done for the head and spine region following a history of head injury.

Results In this study, 120 patients were included, of whom 50.83% ($n=61$) were females and 49.17% ($n=59$) were males. Age ranged from 18 to 70 years with mean age of 43.5 ± 14.08 years. The mean values for linear craniometric parameters of PCF were statistically nonsignificant for different age groups. Statistically significant differences were found for twinning line (TL) ($p<0.0001$), McRae's line (<0.0001), clivus length ($<p<0.0001$), internal occipital protuberence -opisthion line ($p=0.01$), Klaus' index ($p<0.0001$), height of posterior fossa (h) ($p<0.0001$), h/TL ($p=0.028$), when these values were compared for the genders. The measurements of FM transverse diameter, anteroposterior diameter and area were 27.12 ± 1.42 mm (range 23.6–30.1 mm), 30.99 ± 2.23 mm (range 27.6–35.8 mm) and 691.32 ± 30.35 mm^2 (range 632.7–777.7 mm^2). The values of clivus canal angle ($p=0.038$) and clivoodontoid angle ($p=0.012$) were statistically significant when compared for different age groups. The values of Boogard's angle ($p=0.021$) and tentorial slope ($p=0.031$) were statistically significant when these were compared for the genders.

*Correspondence:
Vikrant Yadav
Vikrantyadav473@gmail.com
Full list of author information is available at the end of the article

Conclusions This study described almost all the linear and angular craniometric parameters used in the morphometric analysis of PCF and FM. The findings of this study provide valuable data regarding linear and angular craniometric parameters of PCF and FM which can redefine reference values.

Keywords Basilar invagination, Chiari malformations, Craniometry, Craniovertebral junction, Foramen magnum, Posterior cranial fossa

Introduction

The posterior cranial fossa (PCF) and the foramen magnum (FM) are the key anatomical components of the craniovertebral junction (CVJ), which contain and transmit numerous vital neurovascular structures [1]. The PCF is bounded by the dorsum sellae and the basilar part of the occipital bone anteriorly, the petromastoid part of the temporal bone laterally, the tentorium cerebelli superiorly and the occipital bone posteroinferiorly. The FM in the occipital bone is the largest opening in the PCF [1, 2]. Several important neural elements, i.e. the 7th to 12th cranial nerves, the cervical spinal nerves, the brainstem, the rostral aspect of the spinal cord, the cerebellum and the vermis, as well as various vascular structures such as the vertebral artery and its branches, the meningeal vessels and the venous sinuses are closely associated with the PCF and the FM [3].

The PCF is the site of a variety of neoplastic, vascular, traumatic and degenerative lesions. As it is a rigid and compact space, even a small change in the volume of the PCF or a narrowing of the FM is sufficient to cause life-threatening respiratory and cardiac complications due to compression of the brainstem. Other sequelae of PCF lesions include dysfunction of the lower cranial nerves, limb weakness, hypertonia or hypotonia, hyperreflexia and clonus, etc. [4, 5]. Therefore, a basic knowledge of the radiological anatomy of PCF and FM is of paramount importance for the assessment of associated pathologies and the surgical treatment of these areas.

Various craniometric methods have been developed to measure the linear and angular dimensions of PCF and FM, which have tremendously increased our knowledge of these vital parts [1, 5–7]. Radiological evolutions have further increased the accuracy of measurements of craniometric parameters of PCF and FM, which is indispensable in evaluation of CVJ malformations and surgical approaches to these specific regions [8, 9]. The morphology of the human skull differ in geographically separated populations due to genetic, geographical and environmental variations [10]. India is a large country with huge geographical and environmental variations. The craniometric dimensions of PCF and FM may differ in various regions of India. Since there are no previous craniometric studies of PCF and FM in North India, the aim of this study is to describe different linear and angular craniometric parameters of PCF, FM and surrounding territory based on reconstructed computed tomography (CT) images (as these are commonly used and easily available at a low cost), which may help in our understanding of the morphometry of PCF and FM in this part of India. Additionally, this study also aims to describe each parameters in terms of it's clinical implications in CVJ malformations like Chiari malformations and basilar invagination (BI).

Material and methods

This study was conducted in our tertiary care hospital, situated in northern part of India, from January 2023 to June 2023. 120 patients were included in this study, in which CT screening was done for head and spine regions following history of head injury. All patients included in this study had normal radiological findings on CT scans. Patients with bony, soft tissue or brain parenchymal injuries were excluded from this study. Patient information was anonymized and de-identified prior to analysis. Demographical descriptions and radiological information were recorded for all patients included in this study.

CT imaging protocol

Computed tomography scans were performed using a 128 -slice spiral CT scanner (Discovery Ultra, GE). The rotator time was 0.5 s/rotation with 120 kVp and 200 mAs, the slice thickness was 0.625 mm, the slice interval was 0.625 mm, the field of view was 240 mm × 240 mm, and the matrix size was 512 × 512. Radiological assessments were done in all the patients using reconstructed midsagittal and axial images.

Linear Craniometric evaluation of PCF: We used following linear craniometric parameters:

1. Twinning line (TL)—A distance between the tuberculum sellae and the internal occipital protuberance (IOP)(mm) (Fig. 1a)
2. McRae line (ML)—A distance between the basion and the opisthion (mm) (Fig. 1a)
3. Clivus length (Cl)—A distance between the tip of dorsum the sellae and the basion (mm) (Fig. 1a)
4. IOP-Opisthion (IOP-O) line—A distance between IOP and the opisthion (mm) (Fig. 1b)

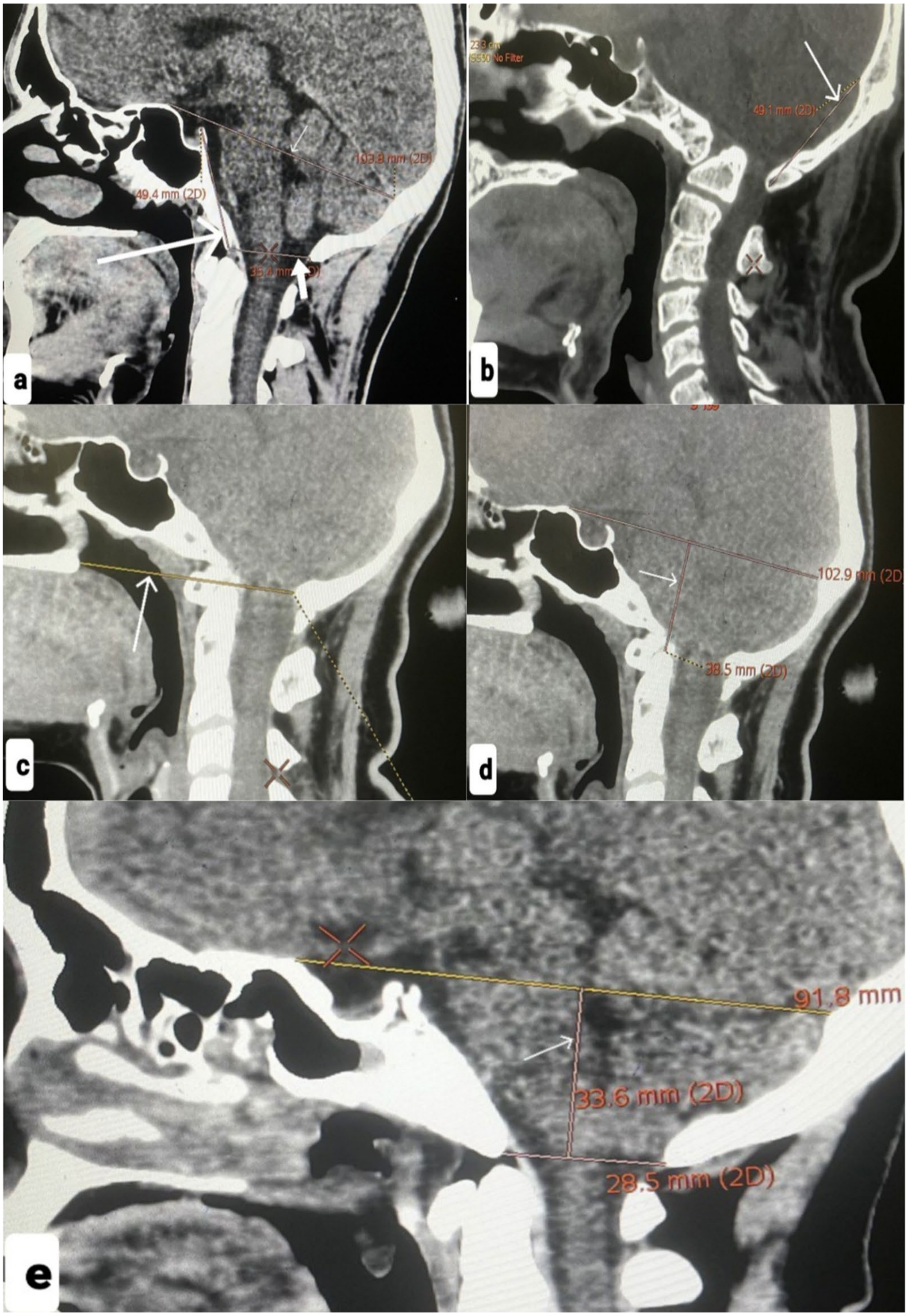

Fig. 1 Midsagittal reconstructed images of the computed tomography scan of the posterior fossa and the craniovertebral junction demonstrating the various linear craniometric parameters. **a** Twinning line (small thin white arrow);connecting the tuberculum sellae and the internal occipital protuberance, McRae's line (thick arrow); connecting the basion to the opisthion, clivus length (long arrow); connecting the tip of the dorsum sellae to the basion. **b** Internal Occipital Protuberance-Opisthion (IOP-O) line (white arrow); connecting internal occipital protuberance to opisthion **c** Chamberlain's line (white arrow); connecting between the posterior end of the hard palate and the opisthion **d** Klaus' index (white arrow); perpendicular distance of the tip of the odontoid process from the twinning line **e** height of the posterior fossa (white arrow); perpendicular distance between McRae's line and the twinning line

5. Chamberlain's line (CL)—A distance between the posterior end of the hard palate and the opisthion (mm) (Fig. 1c)
6. Klaus' index (KI)—A perpendicular distance between the tip of the odontoid process and TL (mm) (Fig. 1d)
7. Height of posterior fossa (h)—A perpendicular distance between ML and TL (mm) (Fig. 1e)
8. Posterior fossa volume (PFV)—PFV (mm^3) was calculated by formula hbc/2; where h is the height of posterior fossa, b is the anteroposterior diameter measured as the distance between the dorsum sellae and IOP, c is the transverse diameter measured as the maximum distance between the points just below the base of the petrous temporal bone.
9. h/TL—measurement of the compensatory anterior growth in the small posterior fossa

Linear Craniometric evaluation of FM: We used the following linear craniometric parameters to analyse FM:

1. Shape of FM—Various shapes of FM were observed on the inferior basal view – oval, round, tetragonal, pentagonal, hexagonal, egg shaped and irregular (Fig. 2a–g)
2. FM transverse diameter (R1)—maximum distance between the basion and the opisthion (mm)
3. FM anteroposterior diameter (R2)—maximum length between the margins of FM measured by drawing a line perpendicular to R1 (mm)
4. FM area-FM area was calculated by Radinsky's formula; πR1R2/4($mm.^2$) (Fig. 2h)

Angular craniometric evaluation of PCF and FM: We used the following angular craniometric parameters to analyse the PCF, FM and surrounding territory (In degrees) (Fig. 3a–j):

1. Basal angle (BA)—The angle between the line connecting the nasion to the dorsum sellae and the line extending from the tip of the dorsum sellae to the tangential surface of the clivus
2. Boogard's angle (BgA)—The angle between the line connecting the tip of the dorsum sellae to the basion and the line from the basion to the opisthion
3. Nasion–Basion-Opisthion (NBO) angle—The angle between the line connecting the nasion, the basion and the opisthion
4. FM angle (FMag)—The angle between Chamberlain's line and McRae's line
5. Clivus canal angle (CCA)—The angle between the line connecting the tip of the dorsum sellae to the basion extrapolating inferiorly and the line between the inferodorsal portions of axis to the most superodorsal part of the odontoid process extrapolating superiorly.
6. Clivopalatal angle (CPA)—The angle between the lines connecting the tip of the dorsum sellae to the basion and the basion to the posterior pole of the hard palate
7. Clivoodontoid angle (COA)—The angle formed at the intersection of a line connecting the tip of the dorsum sellae to the basion extrapolating inferiorly and the one along the long axis of the odontoid process
8. Clivo-Supraocciput angle (CSO)—The angle formed between the intersection of the inferiorly extrapolated lines connecting the dorsum sellae to the basion and the IOP to the opisthion
9. Tentorial slope-The angle between the line along the tentorium and the line connecting IOP and the tip of the opisthion.
10. Tentorial twinning line angle (TtwA)—The angle between the line along the tentorium to IOP and the twinning line.

The data entry was done in the Microsoft Excel spreadsheet, and the final analysis was done with the use of Statistical Package for Social Sciences (SPSS) software, IBM, Chicago, USA, ver 25.0. The presentation of the categorical variables was done in the form of numbers and percentages (%). On the other hand, the quantitative data with a normal distribution were presented as the means ± SD and the data with a non-normal distribution were presented as median with 25th and 75th percentiles (interquartile range).The data normality was checked by using Kolmogorov–Smirnov test. In cases where the data was not normal, we used non parametric tests. The comparison of the variables that were quantitative and not normally distributed in nature was analysed using the Mann–Whitney Test (for two groups) and the Kruskal Wallis test (for more than two groups) and the variables which were quantitative and normally distributed in nature were analysed using Independent t test (for two groups) and ANOVA (for more than two groups). The comparison of the variables, which were qualitative in nature, was analysed using Chi-Square test. If any cell had an expected value of less than five, then Fisher's exact test was used.

For statistical significance, a *p* value of less than 0.05 was considered statistically significant.

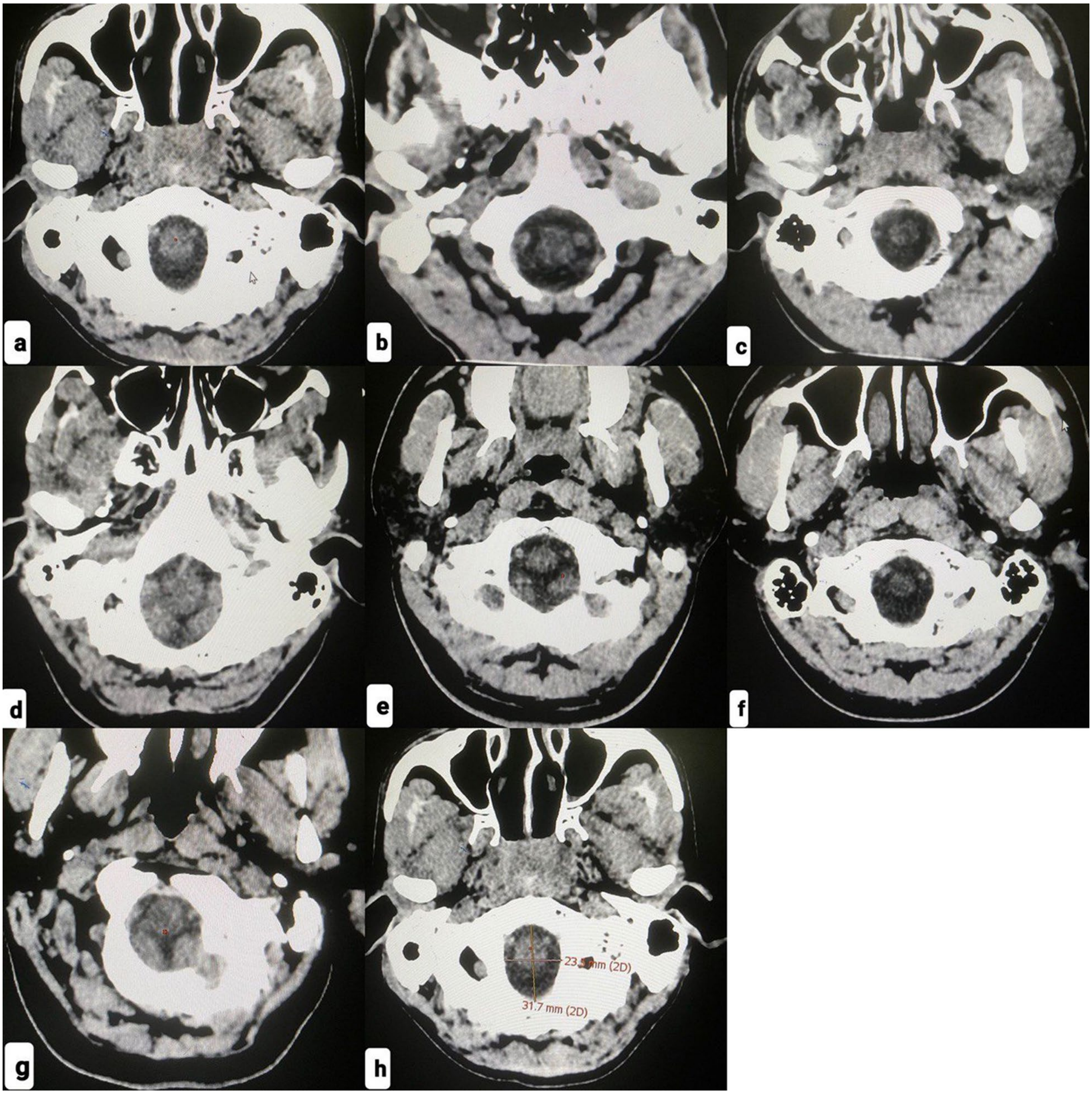

Fig. 2 Axial reconstructed images of computed tomography scan of the posterior fossa demonstrating the various shapes of Foramen magnum. **a** Oval, **b** Round, **c** Tetragonal, **d** Pentagonal, **e** Hexagonal, **f** Egg shaped, **g** Irregular, **h** Measurements of anteroposterior (R1) and transverse diameter (R2) of foramen magnum

Results

In this study, 120 patients were included, of whom 50.83% ($n=61$) were females and 49.17% ($n=59$) were males. The age ranged from 18 to 70 years with a mean age of 43.5 ± 14.08 years. Most of the patients were in the age group 31–40 ($n=37$) (Table 1).

Linear craniometric analysis of PCF

The mean values of the different linear craniometric parameters are given in Table 2.The mean values of all these parameters were statistically nonsignificant for the different age groups (Table 3). Statistically significant differences were found for TL ($p<0.0001$), ML

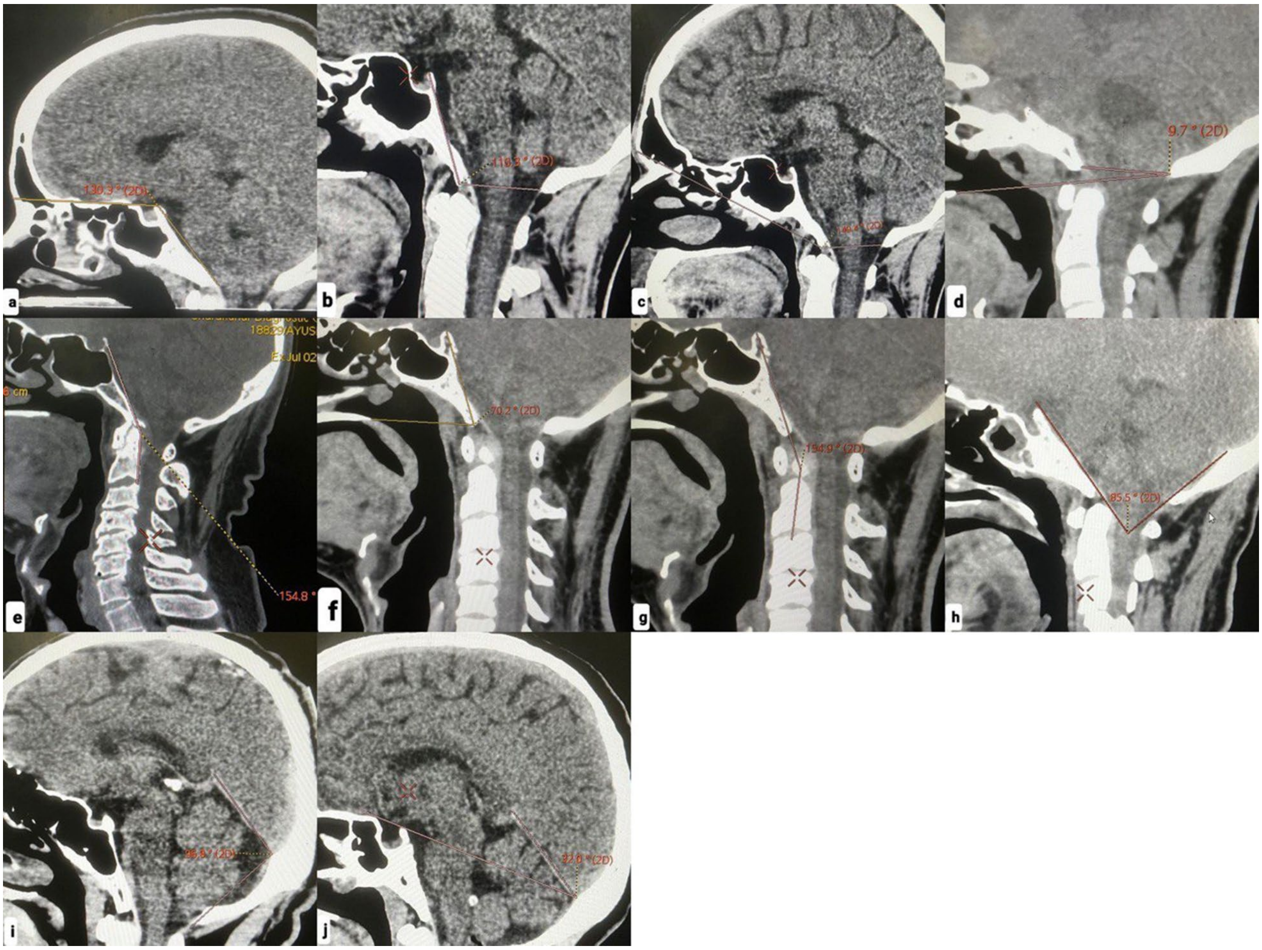

Fig. 3 Midsagittal reconstructed images of computed tomography scan of the posterior fossa and the craniovertebral junction demonstrating the various angular craniometric parameters. **a** Basal angle; angle between line connecting the nasion to the tip of the dorsum sellae and line extending from the tip of the dorsum sellae to the tangential surface of clivus, **b** Boograd's angle; Angle between line connecting the tip of the dorsum sellae to the basion and line from the basion to the opisthion, **c** Nasion–Basion-Opisthion;Angle between line connecting nasion, basion and opisthion, **d** Foramen magnum angle; Angle between Chamberlain's line and McRae's line, **e** Clivus canal angle; Angle between the line connecting the tip of the dorsum sellae to the basion extrapolating inferiorly and line between the inferodorsal portions of the axis to the most superodorsal part of the odontoid process extrapolating superiorly **f** Clivopalatal angle; Angle between lines connecting the tip of the dorsum sellae to the basion and the basion to the posterior pole of the hard palate, **g** Clivoodontoid angle; Angle formed at the intersection of a line connecting tip of dorsum sellae to basion extrapolating inferiorly and the one along the long axis of the odontoid process, **h** Clivo-Supraocciput angle; Angle formed between intersection of inferiorly extrapolated lines connecting the tip of the dorsum sellae to the basion and IOP to the opisthion **i** Tentorial slope; Angle between line along the tentorium to IOP and IOP-O line, **j** Tentorial twinning line angle; Angle between line along the tentorium to IOP and the twinning line

(< 0.0001), Cl ($p < 0.0001$), IOP-O line ($p = 0.01$), KI ($p < 0.0001$), height (h) of posterior fossa ($p < 0.0001$), h/TL ($p = 0.028$), when these values were compared for the genders (Table 4).

Linear craniometric analysis of FM

Different shapes of FM are given in Table 5. The measurements of FM transverse diameter, anteroposterior diameter and area were 27.12 ± 1.42 mm (range 23.6–30.1 mm), 30.99 ± 2.23 mm (range 27.6–35.8 mm) and 691.32 ± 30.35 mm^2 (range 632.7–777.7 mm^2), respectively (Table 6). These measurements were statistically nonsignificant for the various age groups (Table 7), but all these value were statistically significant when compared for the genders ($p = 0.0008$, < 0.0001, 0.043 respectively, for FM transverse diameter, FM anteroposterior diameter and FM area) (Table 8).

Table 1 Demographic analysis

Demographic characteristics	Controls ($n=120$)
Age (years)	
18–30	21 (17.50%)
31–40	37 (30.83%)
41–50	20 (16.67%)
51–60	27 (22.50%)
61–70	15 (12.50%)
Mean ± SD	43.5 ± 14.08
Gender	
Female	61 (50.83%)
Male	59 (49.17%)

Table 2 Analysis of linear Craniometric Parameters of Posterior Cranial Fossa

Linear Craniometric Parameters of Posterior Cranial Fossa	Controls ($n=120$) Mean ± SD	Range
Twinning line (mm){TwL}	97.25 ± 3.21	91.3–104.1
McRae line (mm)	32.26 ± 1.84	28.3–35.9
Clivus length (mm)	41.59 ± 1.99	36.8–49.4
IOP-O line (mm)	43.9 ± 2.03	36.8–49.6
Chamberlain line (mm)	75.51 ± 3.66	67–84
Klaus' index (mm)	44.57 ± 2.27	36.4–49.9
Height of posterior fossa (mm){h}	34.37 ± 1.46	32–36.9
h/TwL	0.35 ± 0.02	–
Posterior fossa volume (cm^3)	162.52 ± 7.64	143.78–175.56

IOP-O: Internal Occipital Protuberance-Opisthion

Angular craniometric analysis of PCF

The measurements of the different angles are given in Table 9.The values of CCA ($p=0.038$) and COA ($p=0.012$) were statistically significant when compared for the different age groups (Table 10). All other angular craniometric parameters were statistically nonsignificant for the different age groups. BgA ($p=0.021$) and TS ($p=0.031$) were statistically significant when these measurements compared for the gender (Table 11). All other measurements were nonsignificant for the genders.

Discussion

The PCF and its surrounding territory incorporate the critical neurovascular structures which include brain stem, cerebellum, cranial nerves, basilar and vertebral arteries, caudal part of ventricular system. FM is the largest opening in the skull bone which transmit medulla and its meninges, vertebral arteries, spinal vessels and ligaments [1–3, 11]. There are normal morphological variations of PCF and FM in the different geographical areas, races and religions. Gender, genetic and environmental factors also influences the morphometry of these parts [7, 10, 12]. A lot of research has been done for the morphometric analysis of PCF, FM and its surrounding territory in different parts of world. The evolution of imaging modalities has increased the precision of our knowledge regarding PCF and FM. We used easily available reconstructed CT images to analyse the morphometry of PCF and FM.

Linear craniometric analysis of PCF and it's clinical implications

Knowledge of measurements of different linear craniometric parameters is necessary for the diagnosis of CVJ and PCF malformations. Chiari malformations are a group of the congenital malformations of CVJ that are frequently associated with the occipital bone dysplasia and other osseous abnormalities like platybasia, BI, clival bone deformity or alterations in the size of PCF [2,

Table 3 Comparison of Linear Craniometric Parameters of Posterior Cranial Fossa for different age groups

Linear Craniometric Parameters of Posterior Cranial Fossa	18–30($n=21$) Mean ± SD	31–40($n=3$) Mean ± SD	41–50($n=20$) Mean ± SD	51–60($n=27$) Mean ± SD	61–70($n=15$) Mean ± SD	Total Mean ± SD	*p* value
Twinning line (mm){TwL}	97.25 ± 3.18	96.92 ± 3.11	98.04 ± 3.57	97.44 ± 3.45	96.68 ± 2.72	97.25 ± 3.21	0.715[a]
McRae's line (mm)	32.51 ± 2.33	32.08 ± 1.57	32.55 ± 1.74	32.26 ± 2	31.98 ± 1.68	32.26 ± 1.84	0.816[a]
Clivus length (mm)	41.54 ± 2.6	41.31 ± 1.7	41.88 ± 1.73	41.74 ± 2.01	41.65 ± 2.2	41.59 ± 1.99	0.863[a]
IOP-O line (mm)	43.37 ± 2.26	43.68 ± 2.15	44.21 ± 1.68	44.39 ± 2.03	43.89 ± 1.81	43.9 ± 2.03	0.432[a]
Chamberlain line (mm)	75.09 ± 3.31	76.06 ± 3.4	75.38 ± 4	75.13 ± 4.19	75.62 ± 3.63	75.51 ± 3.66	0.839[a]
Klaus' index (mm)	44.77 ± 2.9	44.32 ± 1.79	44.49 ± 1.86	44.5 ± 2.68	45.13 ± 2.2	44.57 ± 2.27	0.818[a]
Height of posterior fossa (mm){h}	34.39 ± 1.6	34.15 ± 1.47	34.42 ± 1.55	34.53 ± 1.47	34.56 ± 1.19	34.37 ± 1.46	0.846[a]
Height of supratentorial region (mm){H}	90.77 ± 2.05	91.15 ± 1.81	91.35 ± 2.08	91.98 ± 1.96	90.67 ± 1.98	91.24 ± 1.97	0.173[a]
h/TwL	0.35 ± 0.02	0.35 ± 0.01	0.35 ± 0.02	0.35 ± 0.02	0.36 ± 0.01	0.35 ± 0.02	0.815[a]
Posterior fossa volume (cm^3)	164.47 ± 7.39	161.93 ± 8.23	163.66 ± 5.89	162.96 ± 7.97	158.93 ± 7.51	162.52 ± 7.64	0.247[a]

IOP-O: Internal Occipital Protuberance-Opisthion

[a] ANOVA

Table 4 Comparison of Linear Craniometric Parameters of Posterior Cranial Fossa in between genders

Linear Craniometric Parameters of Posterior Cranial Fossa	Female ($n=61$) Mean ± SD	Male ($n=59$) Mean ± SD	Total Mean ± SD	p value
Twinning line (mm){TwL}	95.89 ± 3.3	98.65 ± 2.44	97.25 ± 3.21	**<.0001[a]**
McRae's line (mm)	31.57 ± 1.83	32.97 ± 1.58	32.26 ± 1.84	**<.0001[a]**
Clivus length (mm)	40.67 ± 1.49	42.53 ± 2.02	41.59 ± 1.99	**<.0001[a]**
IOP-O line (mm)	43.32 ± 1.8	44.5 ± 2.1	43.9 ± 2.03	**0.001[a]**
Chamberlain line (mm)	75.42 ± 3.62	75.61 ± 3.74	75.51 ± 3.66	0.785[a]
Klaus' index (mm)	43.63 ± 2.05	45.54 ± 2.08	44.57 ± 2.27	**<.0001[a]**
Height of posterior fossa (mm){h}	33.57 ± 1.02	35.21 ± 1.38	34.37 ± 1.46	**<.0001[a]**
Height of supratentorial region (mm){H}	91.64 ± 2.03	90.83 ± 1.84	91.24 ± 1.97	**0.024[a]**
h/TwL	0.35 ± 0.02	0.36 ± 0.02	0.35 ± 0.02	**0.028[a]**
Posterior fossa volume (cm^3)	161.53 ± 6.82	163.54 ± 8.35	162.52 ± 7.64	0.151[a]

A significant p value is denoted in bold letters

IOP-O: Internal Occipital Protuberance-Opisthion

[a] Independent t test

Table 5 Analysis of Morphometry of Foramen Magnum

Shapes of Foramen Magnum	Controls ($n=120$)
Oval	27 (22.50%)
Round	24 (20%)
Tetragonal	7 (5.83%)
Pentagonal	8 (6.67%)
Hexagonal	39 (32.50%)
Egg	6 (5%)
Irregular	9 (7.50%)

5, 7, 13–19]. Para axial mesodermal insufficiency during embryological development may be responsible for development of Chiari malformations [20]. The measurement of TL reflects the anteroposterior distance of PCF. In this study, the mean length of TL was 97.25 ± 3.21 mm. In previous literature, the mean length of TL ranges from 84.2 to 93.7 mm [7, 21]. In Chiari malformations, there is growth in the anteroposterior direction to compensate for the small size of the PCF which results in higher values of TL [15, 22]. The length of ML, which

Table 6 Analysis of Linear Craniometric Parameters of Foramen Magnum

Linear Craniometric Parameters of Foramen Magnum	Controls ($n=120$)	Range
Foramen Magnum transverse diameter (mm)	27.12 ± 1.42	23.6–30.1
Foramen Magnum anteroposterior diameter (mm)	30.99 ± 2.23	27.6–35.8
Foramen Magnum area (mm^2)	691.32 ± 30.35	632.7–777.7

Table 7 Comparison of Linear Craniometric Parameters of Foramen magnum in different age groups

Linear Craniometric Parameters of Foramen Magnum	18–30($n=21$) Mean ± SD	31–40($n=37$) Mean ± SD	41–50($n=20$) Mean ± SD	51–60($n=27$) Mean ± SD	61–70($n=15$) Mean ± SD	Total Mean ± SD	p value
Foramen Magnum transverse diameter (mm)	27.03 ± 1.27	27.08 ± 1.63	27.24 ± 1.24	27.59 ± 1.5	26.36 ± 0.78	27.12 ± 1.42	0.111[a]
Foramen Magnum anteroposterior diameter (mm)	31.33 ± 2.45	30.79 ± 2.27	30.97 ± 1.91	31.62 ± 2.27	29.88 ± 1.86	30.99 ± 2.23	0.152[a]
Foramen Magnum area (mm^2)	687.21 ± 35.4	687.19 ± 29.02	698.4 ± 24.11	700.54 ± 32.81	681.21 ± 25.87	691.32 ± 30.35	0.176[a]

[a] ANOVA

Table 8 Comparison of Linear craniometric parameters of Foramen Magnum in between genders

Linear Craniometric Parameters of Foramen Magnum	Female (*n* = 61) Mean ± SD	Male (*n* = 59) Mean ± SD	Total Mean ± SD	*p* value
Foramen Magnum transverse diameter (mm)	26.7 ± 1.27	27.56 ± 1.44	27.12 ± 1.42	**0.0008[a]**
Foramen Magnum anteroposterior diameter (mm)	29.94 ± 1.64	32.07 ± 2.25	30.99 ± 2.23	**< .0001[a]**
Foramen Magnum area (mm^2)	685.82 ± 29.59	697.01 ± 30.31	691.32 ± 30.35	**0.043[a]**

A significant *p* value is denoted in bold letters

[a] Independent t test

Table 9 Analysis of Angular Craniometric Parameters of Posterior Cranial Fossa and Foramen Magnum and Surrounding territory

Angular Craniometric Parameters	Controls (*n* = 120) Mean ± SD	Range
Basal angle (°)	125.92 ± 4.41	118.3–144
Boogard angle (°)	136.89 ± 3.39	129.7–152.1
NBO angle (°)	169.4 ± 2.01	163.5–173.2
Foramen magnum angle (°)	12.88 ± 1.74	9.6–18
Clivo-odontoid angle (°)	145.58 ± 8.78	117.3–157.2
Clivo palatal angle (°)	60.1 ± 5.76	46–71
Clivus canal angle (°)	161.19 ± 9.07	132.1–173.2
Clivus supraocciput angle (°)	77.6 ± 4.52	65.3–93.5
Tentorial slope (°)	88.5 ± 5.87	67–98
Tentorial twinning line angle (°)	34.09 ± 2.12	27.3–40.3

NBO: Nasion Basion Opisthion

a gives measure of wideness of FM, varies from 32.3 to 36.21 mm [21, 23]. Although in CVJ malformations, it's significance remains inconspicuous, as previous studies failed to establish the significance between the length of ML and CVJ malformations., but usually measurements of ML remains higher in Chiari malformations. The mean length of ML was 32.26 mm in this study. The length of CL is not well documented in the literature. In this study, the mean length of CL was 75.51 ± 3.66 mm. The mean length of clivus (Cl) and KI (Fig. 4a), which are measures of the size of the basiocciput, vary from 40.4 to 47.22 mm and 38 to 40.9 mm, respectively, in the normal population [5, 7, 22, 24–27]. In this study, it was 41.59 ± 1.99 mm and 44.57 ± 2.27 mm, respectively. Mean values of Cl and KI is lesser in the patients with Chiari malformations and BI than in the normal population.The IOP-O line is a measure of supraocciput, and it's mean length varies from 40.9 to 46.8 mm in the normal population [7, 26]. In this study, the mean length of IOP-O line was 43.9 ± 2.03 mm. The height of the posterior fossa is a measure of the shallowness of the posterior fossa, which varies from 30.3 to 35.2 mm in various studies, probably due to the choice of different landmarks. A decreased height of the posterior fossa denotes a smaller posterior fossa volume (Fig. 4b) which is associated with Chiari malformations [7, 12, 27]. In this study, it's value was 34.37 ± 1.46 mm. h/TwL is considered compensatory growth of PCF in the forward

Table 10 : Comparison of Angular Craniometric Parameters of Posterior Cranial Fossa, Foramen Magnum and surrounding territory in different age groups

Angular Craniometric Parameters	18–30(*n* = 21) Mean ± SD	31–40(*n* = 37) Mean ± SD	41–50(*n* = 20) Mean ± SD	51–60 (*n* = 27) Mean ± SD	61–70 (*n* = 15) Mean ± SD	Total Mea± SD	*p* value
Basal angle (°)	125.66 ± 3.14	125.88 ± 4.5	125.14 ± 4.37	127.03 ± 5.49	125.42 ± 3.72	125.92 ± 4.41	0.633[a]
Boogard angle (°)	137.4 ± 4.34	137.54 ± 3.43	135.12 ± 2.43	137 ± 2.84	136.74 ± 3.44	136.89 ± 3.39	0.118[a]
NBO angle (°)	169.31 ± 2.38	169.39 ± 2.09	169.75 ± 1.24	169.45 ± 2.08	169.03 ± 2.1	169.4 ± 2.01	0.884[a]
Foramen Magnum angle (°)	12.5 ± 1.13	12.5 ± 1.54	13.57 ± 2.25	13.2 ± 1.99	12.87 ± 1.47	12.88 ± 1.74	0.148[a]
Clivo-odontoid angle (°)	147.17 ± 7.72	143.98 ± 9.23	150.5 ± 4.97	142.19 ± 11	146.84 ± 4.86	145.58 ± 8.78	**0.012[a]**
Clivo palatal angle (°)	59.83 ± 5.82	59.48 ± 5.32	60.76 ± 5.36	59.82 ± 6.35	61.59 ± 6.5	60.1 ± 5.76	0.778[a]
Clivus canal angle (°)	162.72 ± 7.85	159.95 ± 9.74	165.62 ± 5.11	157.83 ± 11.39	162.23 ± 5.65	161.19 ± 9.07	**0.038[a]**
Clivus supraocciput angle (°)	77.82 ± 5.71	77.31 ± 3.76	76.86 ± 4.65	78.66 ± 4.07	77.09 ± 5.23	77.6 ± 4.52	0.671[a]
Tentorial slope (°)	87.09 ± 5.94	88.42 ± 5.44	90.36 ± 6.07	87.81 ± 6.5	89.43 ± 5.26	88.5 ± 5.87	0.416[a]
Tentorial twinning line angle (°)	34.24 ± 2.25	33.69 ± 2.47	34.54 ± 1.66	34.21 ± 2.07	34.06 ± 1.68	34.09 ± 2.12	0.666[a]

A significant *p* value is denoted in bold letters

NBO: Nasion Basion Opisthion

[a] ANOVA

Table 11 Comparison of Angular Craniometric Parameters of Posterior Cranial Fossa, Foramen Magnum and surrounding territory in between genders

Angular Craniometric Parameters	Female ($n = 61$) Mean ± SD	Male ($n = 59$) Mean ± SD	Total Mean ± SD	p value
Basal angle (°)	125.68 ± 5.24	126.17 ± 3.37	125.92 ± 4.41	0.542[a]
Boogard angle (°)	136.19 ± 3.02	137.62 ± 3.63	136.89 ± 3.39	**0.021[a]**
NBO angle (°)	169.07 ± 1.93	169.75 ± 2.04	169.4 ± 2.01	0.061[a]
Foramen Magnum angle (°)	12.97 ± 1.7	12.79 ± 1.79	12.88 ± 1.74	0.575[a]
Clivo-odontoid angle (°)	146.72 ± 8.63	144.4 ± 8.84	145.58 ± 8.78	0.149[a]
Clivo palatal angle (°)	60.23 ± 6.23	59.95 ± 5.27	60.1 ± 5.76	0.79[a]
Clivus canal angle (°)	162.11 ± 8.82	160.24 ± 9.29	161.19 ± 9.07	0.259[a]
Clivus supraocciput angle (°)	77.29 ± 4.33	77.92 ± 4.73	77.6 ± 4.52	0.451[a]
Tentorial slope (°)	89.63 ± 5.82	87.33 ± 5.73	88.5 ± 5.87	**0.031[a]**
Tentorial twinning line angle (°)	34.14 ± 2.09	34.04 ± 2.17	34.09 ± 2.12	0.794[a]

A significant p value is denoted in bold letters

NBO: Nasion Basion Opisthion

[a] Independent t test

direction in the case of small sized PCF [7, 28], although literature regarding the significance of this parameter remains scarce. Karagöz F, et al., in their study, showed that the value of h/TwL was reduced (0.26) in patients with Chiari malformations compared to the normal population (0.32) [7]. In this study, the mean value of h/TwL ratio was 0.35 ± 0.02. Various studies have been done to define the values of PFV based on the different automated and manual methods. The range of the values of PFV varies widely, which may be attributed to the differences in the imaging modalities and the possible differences in the segmentation protocols, or to the landmarks used in the measurement protocol [1, 2, 5, 7, 12, 29]. In this study, the mean PFV was 162 ± 7.64 cm^3. Chiari malformations and BI are most of the times associated with the smaller PCF.

Linear craniometric analysis of FM and its clinical implications

Measurements of the FM hold substantial importance in approaching the lesions occupying the PCF and CVJ region.During surgical procedures, information about the morphometry, morphology, and variations of the FM may affect the surgical outcome.

The Shape of FM has immense clinical significance regarding various surgical approaches. Previous studies have reported differences in the frequency of shapes of FM. It may due to geographical variations, gender and racial differences, etc. The commonest shape of FM described in most of the literatures is oval [30–34]. However, in this study, the most common shape of FM was hexagonal (32.50%), followed by oval (22.50%). Other shapes of FM were round (20%), tetragonal (5.83%), pentagonal (6.67%), irregular (7.50%) and egg shaped (5%).

The anteroposterior and transverse diameters of FM are the other valuable parameters used in analysing variations of the morphometry of FM. In literature, the anteroposterior and transverse diameters of FM range from 25 to 37 mm and 24 to 35 mm, respectively [5, 7, 12, 30, 31, 34, 35]. In this study, these measurements were 30.99 ± 2.23 mm and 27.12 ± 1.42 mm, respectively. The measurement of the area of FM is another morphometric tool to analyse FM, whose value of which ranges from 385 to 779 mm^2, as described in different studies. In this study, it's value was 691 ± 30.35 mm^2. Usually, there are no differences in the size of FM in different age groups, but males have a larger configuration of FM than females [30–37]. Although patients with Chiari malformations have larger dimensions of FM due to compensatory growth in the anteroposterior direction, some studies have found no significance in both [37–39]. Muthukumar et al. described importance of anatomical knowledge of FM as necessary for surgical approaches like the transcondylar approach, where drilling of the posterior margin is important to access lesions [31].

Angular craniometric analysis of PCF, FM and surrounding territory and its clinical implications

Evaluation of the craniocervical angles of PCF, FM and CVJ is necessary, as the cranial angles of PCF directly influence the angular geometry of CVJ and consequently the whole vertebral column [6]. BA is routinely used to asses the flattening of skull base, i.e., platybasia. In literature, it's value ranges from 125° to 143° [40]. The mean value in the previous studies varies due to the use of the

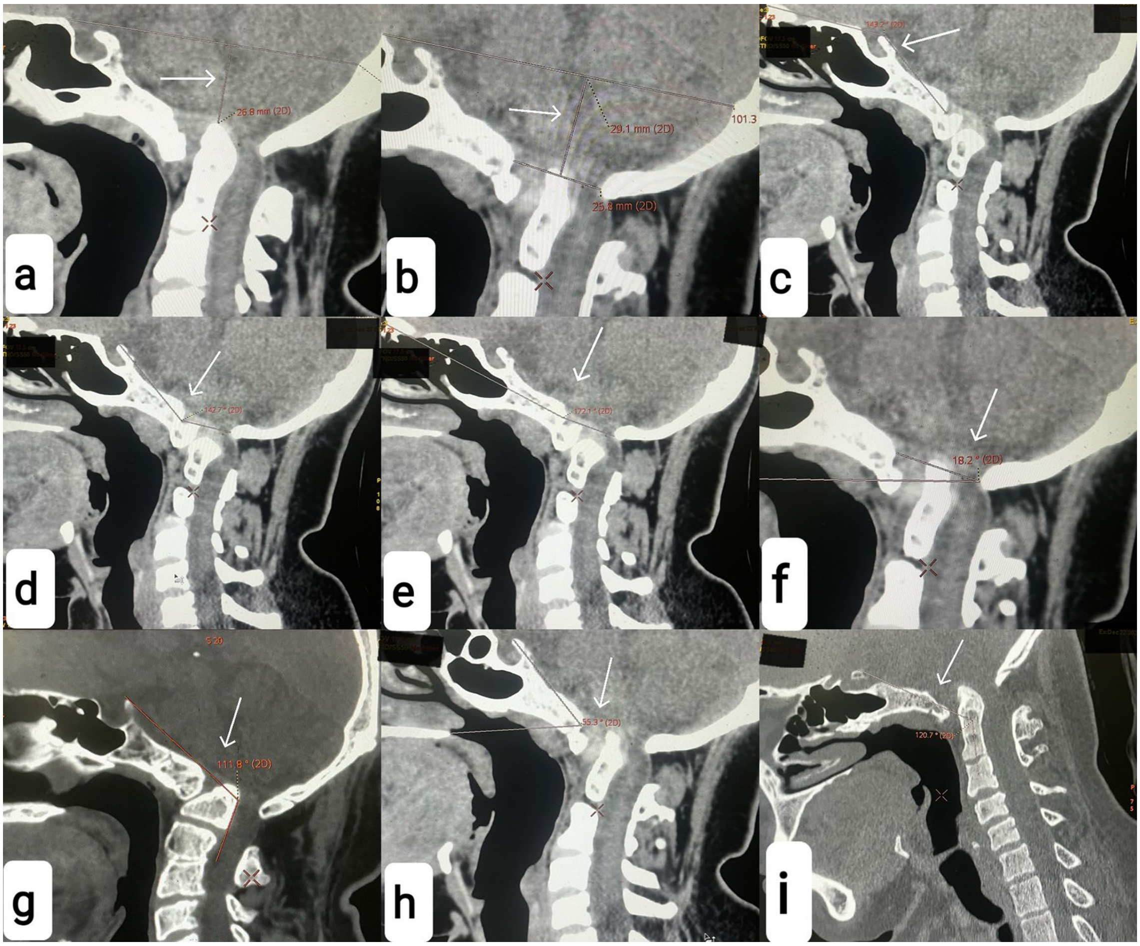

Fig. 4 Midsagittal reconstructed images of computed tomography scan of the posterior fossa and the craniovertebral junction demonstrating the measurements of various craniometric parameters in patients with craniovertebral junction malformations. **a** Klaus' index—26.8 mm (decreased), **b** height of posterior fossa—29.1 mm (decreased), **c** Basal angle—143.2°(increased), **d** Boogard angle—142.7° (increased), **e** Nasion Basion Opisthion angle—172.1 (increased), **f** Foramen Magnum Angle—18.2° (increased), **g** Clivus Canal angle-111.8°(increased), **h** Clivopalatal angle—55.3(decreased), **i** Clivoodontoid angle – 120.7°(decreased)

different imaging modalities or ambiguities in the location of landmarks [40, 41]. In this study, the mean value of BA was 125.92° ± 4.41°. Ferreira et al. stated that BA > 129 is defined as platybasia with mean value of 116.5° in normal population (Fig. 4c) [41]. BgA and NBO angles are also used for the evaluation of platybasia (Fig. 4d, e). The mean value of BgA ranges from 126°-137° in the normal population [6, 7]. In this study, the mean value of BgA was 136.89° ± 3.39°. Botelho et al. found wider BgA in patients with BI (172°) and Chiari malformations (136°) than the control group of the normal population (126° ± 15.26°) [7]. NBO Angle values vary between 162° and 165° [7, 23, 42]. However, in this study, the mean value of NBO angle was 169.4° ± 2.01°, which was slightly higher than stated in the previous literature. Measurements of BA, BgA and NBO angles are helpful in diagnosing CVJ malformations like BI and Chiari malformations. All these angles have greater values when measured in the patients with CVJ malformations [6, 7, 23, 41, 42, 44]. A few more angles have been reiterated to complement the diagnosis of BI; FMag is the one of them (Fig. 4f). It's values ranges from 6.21°-11.6° in the normal population, as described in the previous studies. Nascimento et al. Found a much higher value of FMag (25.9° ± 9.3°) in patients with BI than in the normal population [43, 45]. In this study, the mean value of FMag was 12.88 ± 1.74, which was slightly higher than stated in the previous literature. CCA, CPA, COA and CSO are another set of angles that are useful in complementing the diagnosis of CVJ malformations but literature regarding their data and diagnostic value remains scarce. Measurements of these angles are poorly understood and vary in the previous literatures due to the consideration of the different landmarks or imaging modalities [46–48]. In this study, the mean values of

CCA, CPA, COA, CSO were 161.19° ± 9.07°, 60.1° ± 5.76°, 145.58° ± 8.78° and 77.6° ± 4.52°, respectively. Usually, patients with BI, CCA, CPA, COA have lower values the than the normal population (Fig. 4 g–i), but the value of CSO is greater [46–49]. Ma et al. evaluated CPA, COA and CCA and found cut-off values for diagnosing BI, respectively, at 53.5°, 123.5°, 138.5° [47]. D'AAddario et al. used CSO measurement in the evaluation of fetal posterior fossa and type 2 Chiari malformations, as the values of CSO angle remain constant through out the gestational age.They found that values of CSO angle decreases in patients with fetal ventriculomegaly related to Chiari malformations [50]. Tentorial slope and TtwA are also measured to asses platybasia [7]. In this study, the mean value of the tentorial slope and TtwA were 88.5° ± 5.87° and 34.09° ± 2.12°, respectively. Rehder et al. established tentorial slope as a imaging biomarker of the fetal posterior cranial fossa development [51]. Tentorial slope also and TtwA tend to be greater in value in patients with Chiari malformations, but pertaining literature remains controversial [2, 7, 51–53].

To our best knowledge, no previous study has been published in the literature regarding the descriptive analysis of the morphometry of PCF and FM in the population of the North India. We herein describe different linear and angular craniometric parameters of PCF and FM along with their values in this group of the normal population. These values can be taken as reference values while comparing these parameters in patients with CVJ malformations.

Limitations

This study is not without limitations. First, compared with other studies, the sample size is not large enough. Second, we didn't compare the values of different linear and angular craniometric parameters of this part of India with some other territory of India, which could establish the geographical differences between these parameters. Third, we couldn't find the definitive cause of differences in measurements of some parameters. We are looking forward to performing future studies with larger sample size and comparing these findings with those of other geographical regions of India.

Conclusions

The fundamental knowledge of the morphology of PCF and FM is critical in the evaluation of CVJ malformations and surgically approaching these areas. Linear craniometric parameters like ML, CL and KI are commonly used in the evaluation of BI. Assessment of TL, height of posterior cranial fossa, IOP-O length, clival length and PCF volume are important in making the diagnosis of Chiari malformations. BA, BgA, NBO are the measures of platybasia and are extensively used in making the diagnosis of BI. FMag, CCA and CPA are relatively newer parameters that are helpful in evaluating BI. This study described almost all the linear and angular craniometric parameters used in the morphometric analysis of PCF and FM. Findings of this study provide the valuable data regarding the linear and angular craniometric parameters of PCF and FM which could redefine the reference values.

Abbreviations

PCF	Posterior cranial fossa
FM	Foramen magnum
CVJ	Craniovertebral junction
TL	Twinning line
ML	McRae's line
CL	Chamberlain's line
IOP-O	Internal occipital protuberance-opisthion
KI	Klaus' index
BA	Basal angle
BgA	Boogard's angle
FMag	Foramen magnum angle
CCA	Clivus canal angle
CPA	Clivo palatal angle
COA	Clivo odontoid angle
CSO	Clivo supraocciput angle
TtwA	Tentorial twinning line angle

Acknowledgements

Special gratitude to Professor Kulwant Singh for his immaculate guidance in preparing this article

Author contributions

Data acquisition was performed by VY; analysis of data was conducted by AS and RS; drafting of the manuscript was written by MM and RP; conception and design was provided by RS; critical revision was done by AS. All authors read and approved the final manuscript.

Funding

All patients in this study were evaluated in the hospital for free.

Availability of data and materials

All data that support the findings of this study are available from the neurosurgery department of Institute of Medical Sciences, Banaras Hindu University. Data are however available from the author when requested with permission.

Declarations

Ethics approval and consent to participate

This study was conducted after getting ethical clearance from local institutional ethical committee members. Consent for participation was obtained from each patient prior to the study.

Consent for publication

Not applicable. We confirm that all data incorporated into this study are anonymized.

Competing interests

The authors declare that they have no competing interests.

Author details

[1]Department of Neurosurgery, Institute of Medical Sciences, Banaras Hindu University, Varanasi, Uttar Pradesh, India.

Received: 14 December 2023 Accepted: 5 January 2024
Published online: 26 February 2024

References

1. Oberman DZ, Baldoncini M, Rabelo NN, Ajler P. Morphometric analysis of posterior cranial fossa and surgical implications. J Craniovertebr Junction Spine. 2021;12(2):178–82. https://doi.org/10.4103/jcvjs.jcvjs_205_20.
2. Nishikawa M, Sakamoto H, Hakuba A, Nakanishi N, Inoue Y. Pathogenesis of Chiari malformation: a morphometric study of the posterior cranial fossa. J Neurosurg. 1997;86(1):40–7. https://doi.org/10.3171/jns.1997.86.1.0040.
3. Wen HT, Rhoton AL Jr, Katsuta T, de Oliveira E. Microsurgical anatomy of the transcondylar, supracondylar, and paracondylar extensions of the far-lateral approach. J Neurosurg. 1997;87(4):555–85. https://doi.org/10.3171/jns.1997.87.4.0555.
4. Bagley CA, Pindrik JA, Bookland MJ, Camara-Quintana JQ, Carson BS. Cervicomedullary decompression for foramen magnum stenosis in achondroplasia. J Neurosurg. 2006;104(3 Suppl):166–72. https://doi.org/10.3171/ped.2006.104.3.166.
5. Iqbal S, Robert AP, Mathew D. Computed tomographic study of posterior cranial fossa, foramen magnum, and its surgical implications in Chiari malformations. Asian J Neurosurg. 2017;12(3):428–35. https://doi.org/10.4103/1793-5482.175627.
6. Botelho RV, Ferreira ED. Angular craniometry in craniocervical junction malformation. Neurosurg Rev. 2013;36(4):603–10. https://doi.org/10.1007/s10143-013-0471-0.
7. Karagöz F, Izgi N, Kapíjcíjoğlu SS. Morphometric measurements of the cranium in patients with Chiari type I malformation and comparison with the normal population. Acta Neurochir (Wien). 2002;144(2):165–71. https://doi.org/10.1007/s007010200020.
8. Wang S, Zhang D, Wu K, Fan W, Fan T. Potential association among posterior fossa bony volume and crowdedness, tonsillar hernia, syringomyelia, and CSF dynamics at the craniocervical junction in Chiari malformation type I. Front Neurol. 2023;14:1069861. https://doi.org/10.3389/fneur.2023.1069861.
9. Vazquez S, Dominguez JF, Das A, et al. Treatment of Chiari malformations with craniovertebral junction anomalies: where do we stand today? World Neurosurg X. 2023;20:100221. https://doi.org/10.1016/j.wnsx.2023.100221.
10. Relethford JH. Population-specific deviations of global human craniometric variation from a neutral model. Am J Phys Anthropol. 2010;142(1):105–11. https://doi.org/10.1002/ajpa.21207.
11. Govsa F, Ozer MA, Celik S, Ozmutaf NM. Three-dimensional anatomic landmarks of the foramen magnum for the craniovertebral junction. J Craniofac Surg. 2011;22(3):1073–6. https://doi.org/10.1097/SCS.0b013e3182107610.
12. Kanodia G, Parihar V, Yadav YR, Bhatele PR, Sharma D. Morphometric analysis of posterior fossa and foramen magnum. J Neurosci Rural Pract. 2012;3(3):261–6. https://doi.org/10.4103/0976-3147.102602.
13. Goel A. Basilar invagination, Chiari malformation, syringomyelia: a review. Neurol India. 2009;57(3):235–46. https://doi.org/10.4103/0028-3886.53260.
14. Donnally III CJ, Munakomi S, Varacallo M. Basilar Invagination. [Updated 2023 Feb 12]. In: StatPearls [Internet]
15. Schady W, Metcalfe RA, Butler P. The incidence of craniocervical bony anomalies in the adult Chiari malformation. J Neurol Sci. 1987;82(1–3):193–203. https://doi.org/10.1016/0022-510x(87)90018-9.
16. Vega A, Quintana F, Berciano J. Basichondrocranium anomalies in adult Chiari type I malformation: a morphometric study. J Neurol Sci. 1990;99(2–3):137–45. https://doi.org/10.1016/0022-510x(90)90150-l.
17. Yan H, Han X, Jin M, et al. Morphometric features of posterior cranial fossa are different between Chiari I malformation with and without syringomyelia. Eur Spine J. 2016;25(7):2202–9. https://doi.org/10.1007/s00586-016-4410-y.
18. Stovner LJ, Bergan U, Nilsen G, Sjaastad O. Posterior cranial fossa dimensions in the Chiari I malformation: relation to pathogenesis and clinical presentation. Neuroradiology. 1993;35(2):113–8. https://doi.org/10.1007/BF00593966.
19. Botelho RV, Botelho PB, Hernandez B, Sales MB, Rotta JM. Association between brachycephaly, chiari malformation, and basilar invagination. J Neurol Surg A Cent Eur Neurosurg. 2023;84(4):329–33. https://doi.org/10.1055/s-0041-1739503.
20. Marín-Padilla M. Cephalic axial skeletal-neural dysraphic disorders: embryology and pathology. Can J Neurol Sci. 1991;18(2):153–69. https://doi.org/10.1017/s0317167100031632.
21. Liu Z, Hao Z, Hu S, Zhao Y, Li M. Predictive value of posterior cranial fossa morphology in the decompression of Chiari malformation type I: a retrospective observational study. Medicine (Baltimore). 2019;98(19):e15533. https://doi.org/10.1097/MD.0000000000015533.
22. Diniz JM, Botelho RV. The role of clivus length and cranial base flexion angle in basilar invagination and Chiari malformation pathophysiology. Neurol Sci. 2020;41(7):1751–7. https://doi.org/10.1007/s10072-020-04248-1.
23. Alkoç OA, Songur A, Eser O, et al. Stereological and morphometric analysis of MRI Chiari malformation type-1. J Korean Neurosurg Soc. 2015;58(5):454–61. https://doi.org/10.3340/jkns.2015.58.5.454.
24. Dogan GM, Sigirci A, Tetik B, Pasahan R, Onal C, Arslan AK. Comparison of posterior cranial fossa morphometric measurements in Chiari type I patients with and without syrinx cavity on magnetic resonance imaging. Pol J Radiol. 2022;87:e694–700. https://doi.org/10.5114/pjr.2022.123895.
25. Nwotchouang BST, Eppelheimer MS, Ibrahimy A, et al. Clivus length distinguishes between asymptomatic healthy controls and symptomatic adult women with Chiari malformation type I. Neuroradiology. 2020;62(11):1389–400. https://doi.org/10.1007/s00234-020-02453-5.
26. Nishikawa M, Bolognese PA, Kula RW, Ikuno H, Ohata K. Pathogenesis and classification of Chiari malformation type I based on the mechanism of ptosis of the brain stem and cerebellum: a morphometric study of the posterior cranial fossa and craniovertebral Junction. J Neurol Surg B Skull Base. 2021;82(3):277–84. https://doi.org/10.1055/s-0039-1691832.
27. Bogdanov EI, Heiss JD, Mendelevich EG, Mikhaylov IM, Haass A. Clinical and neuroimaging features of "idiopathic" syringomyelia. Neurology. 2004;62(5):791–4. https://doi.org/10.1212/01.wnl.0000113746.47997.ce.
28. Nyland H, Krogness KG. Size of posterior fossa in Chiari type 1 malformation in adults. Acta Neurochir (Wien). 1978;40(3–4):233–42. https://doi.org/10.1007/BF01774749.
29. Bagci AM, Lee SH, Nagornaya N, Green BA, Alperin N. Automated posterior cranial fossa volumetry by MRI: applications to Chiari malformation type I. AJNR Am J Neuroradiol. 2013;34(9):1758–63. https://doi.org/10.3174/ajnr.A3435.
30. Natsis K, Piagkou M, Skotsimara G, Piagkos G, Skandalakis P. A morphometric anatomical and comparative study of the foramen magnum region in a Greek population. Surg Radiol Anat. 2013;35(10):925–34. https://doi.org/10.1007/s00276-013-1119-z.
31. Muthukumar N, Swaminathan R, Venkatesh G, Bhanumathy SP. A morphometric analysis of the foramen magnum region as it relates to the transcondylar approach. Acta Neurochir (Wien). 2005;147(8):889–95. https://doi.org/10.1007/s00701-005-0555-x.
32. Alaftan M, Alkhater S, Alhaddad F, et al. Morphological variations and morphometry details of the foramen ovale in the Saudi population: a retrospective radiological study. J Med Life. 2023;16(3):458–62. https://doi.org/10.25122/jml-2022-0265.
33. Prakash KG, Saniya K, Honnegowda TM, Ramkishore HS, Nautiyal A. Morphometric and anatomic variations of foramen ovale in human skull and its clinical importance. Asian J Neurosurg. 2019;14(4):1134–7. https://doi.org/10.4103/ajns.AJNS_243_19.
34. Bahşi İ, Adanır SS, Orhan M, et al. Anatomical evaluation of the foramen magnum on cone-beam computed tomography images and review of literature. Cureus. 2021;13(11):e19385. https://doi.org/10.7759/cureus.19385.
35. Tubbs RS, Elton S, Grabb P, Dockery SE, Bartolucci AA, Oakes WJ. Analysis of the posterior fossa in children with the Chiari 0 malformation. Neurosurgery. 2001;48(5):1050–5. https://doi.org/10.1097/00006123-200105000-00016.
36. Gardner WJ, Goodall RJ. The surgical treatment of Arnold-Chiari malformation in adults; an explanation of its mechanism and importance of encephalography in diagnosis. J Neurosurg. 1950;7(3):199–206. https://doi.org/10.3171/jns.1950.7.3.0199.

37. Burdan F, Szumiło J, Walocha J, et al. Morphology of the foramen magnum in young Eastern European adults. Folia Morphol (Warsz). 2012;71(4):205–16.
38. Bogdanov EI, Faizutdinova AT, Heiss JD. The small posterior cranial fossa syndrome and chiari malformation type 0. J Clin Med. 2022;11(18):5472. https://doi.org/10.3390/jcm11185472.
39. Furtado SV, Thakre DJ, Venkatesh PK, Reddy K, Hegde AS. Morphometric analysis of foramen magnum dimensions and intracranial volume in pediatric Chiari I malformation. Acta Neurochir (Wien). 2010;152(2):221–7. https://doi.org/10.1007/s00701-009-0480-5.
40. Koenigsberg RA, Vakil N, Hong TA, et al. Evaluation of platybasia with MR imaging. AJNR Am J Neuroradiol. 2005;26(1):89–92.
41. Ferreira JA, Botelho RV. Determination of normal values of the basal angle in the era of magnetic resonance imaging [published correction appears in World Neurosurg. 2020 Apr;136:480]. World Neurosurg. 2019;132:363–7. https://doi.org/10.1016/j.wneu.2019.09.056.
42. Adam AM. Skull radiograph measurements of normals and patients with basilar impression; use of Landzert's angle. Surg Radiol Anat. 1987;9(3):225–9. https://doi.org/10.1007/BF02109633.
43. Nascimento JJC, Silva LM, Ribeiro ECO, Neto EJS, Araújo-Neto SA, Diniz PRB. Foramen magnum angle: a new parameter for basilar invagination of type B. World Neurosurg. 2021;152:121–3. https://doi.org/10.1016/j.wneu.2021.06.028.
44. Silva ATPB, Silva LTPB, Vieira AENR, et al. Craniometric parameters for the evaluation of platybasia and basilar invagination on magnetic resonance imaging: a reproducibility study. Radiol Bras. 2020;53(5):314–9. https://doi.org/10.1590/0100-3984.2019.0068.
45. Jian Q, Zhang B, Jian F, Bo X, Chen Z. Basilar invagination: a tilt of the foramen magnum [published correction appears in World Neurosurg. 2022 Nov;167:255]. World Neurosurg. 2022;164:e629–35. https://doi.org/10.1016/j.wneu.2022.05.027.
46. Nagashima C, Kubota S. Craniocervical abnormalities. Modern diagnosis and a comprehensive surgical approach. Neurosurg Rev. 1983;6(4):187–97. https://doi.org/10.1007/BF01743100.
47. Ma L, Guo L, Li X, et al. Clivopalate angle: a new diagnostic method for basilar invagination at magnetic resonance imaging. Eur Radiol. 2019;29(7):3450–7. https://doi.org/10.1007/s00330-018-5972-3.
48. Xu S, Gong R. Clivodens Angle: A New Diagnostic Method for Basilar Invagination at Computed Tomography. Spine (Phila Pa 1976). 2016;41(17):1365–71. https://doi.org/10.1097/BRS.0000000000001509.
49. Basaran R, Efendioglu M, Senol M, Ozdogan S, Isik N. Morphometric analysis of posterior fossa and craniovertebral junction in subtypes of Chiari malformation. Clin Neurol Neurosurg. 2018;169:1–11. https://doi.org/10.1016/j.clineuro.2018.03.017.
50. D'Addario V, Pinto V, Del Bianco A, et al. The clivus-supraocciput angle: a useful measurement to evaluate the shape and size of the fetal posterior fossa and to diagnose Chiari II malformation. Ultrasound Obstet Gynecol. 2001;18(2):146–9. https://doi.org/10.1046/j.1469-0705.2001.00409.x.
51. Rehder R, Yang E, Cohen AR. Variation of the slope of the tentorium during childhood. Childs Nerv Syst. 2016;32(3):441–50. https://doi.org/10.1007/s00381-015-2899-8.
52. Kao SC, Waziri MH, Smith WL, Sato Y, Yuh WT, Franken EA Jr. MR imaging of the craniovertebral junction, cranium, and brain in children with achondroplasia. AJR Am J Roentgenol. 1989;153(3):565–9. https://doi.org/10.2214/ajr.153.3.565.
53. Milhorat TH, Chou MW, Trinidad EM, et al. Chiari I malformation redefined: clinical and radiographic findings for 364 symptomatic patients. Neurosurgery. 1999;44(5):1005–17. https://doi.org/10.1097/00006123-199905000-00042.

Publisher's Note